ACS Chemical Neuroscience

Research Article

pubs.acs.org/chemneuro

Continuous Online Microdialysis Using Microfluidic Sensors: Dynamic Neurometabolic Changes during Spreading Depolarization

Michelle L. Rogers,[†,∥] Delphine Feuerstein,[‡,∥] Chi Leng Leong,[†] Masatoshi Takagaki,[‡] Xize Niu,[§] Rudolf Graf,[‡] and Martyn G. Boutelle*[,†]

[†]Department of Bioengineering, Imperial College, London, United Kingdom

[‡]Max Planck Institute for Neurological Research, Cologne, Germany

[§]Engineering and the Environment, University of Southampton, Southampton, United Kingdom

ABSTRACT: Microfluidic glucose biosensors and potassium ion selective electrodes were used in an in vivo study to measure the neurochemical effects of spreading depolarizations (SD), which have been shown to be detrimental to the injured human brain. A microdialysis probe implanted in the cortex of rats was connected to a microfluidic PDMS chip containing the sensors. The dialysate was also analyzed using our gold standard, rapid sampling microdialysis (rsMD). The glucose biosensor performance was validated against rsMD with excellent results. The glucose biosensors successfully monitored concentration changes, in response to SD wave induction, in the range of 10−400 μM with a second time-resolution. The data show that during a SD wave, there is a time delay of 62 ± 24.8 s (n = 4) between the onset of the increase in potassium and the decrease in glucose. This delay can be for the first time demonstrated, thanks to the high-temporal resolution of the microfluidic sensors sampling from a single tissue site (the microdialysis probe), and it indicates that the decrease in glucose is due to the high demand of energy required for repolarization.

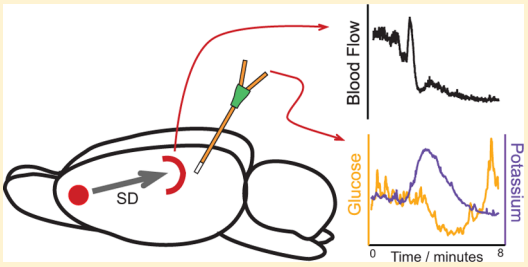

KEYWORDS: *Microfluidic, biosensor, microdialysis, real-time, spreading depolarization*

Traumatic brain injury (TBI) has been described as a silent epidemic by an editorial in *Lancet Neurology* journal.[1] This stark judgment is based upon facts such as the annual United States incidence of TBI (390−445/100 000 population) being higher than that of breast cancer (120/100 000 population),[2] and an estimated direct and indirect cost of $60 billion in 2000.[3]

TBI may take many forms including intracerebral hemorrhage, subarachnoid hemorrhage, cerebral contusion, and axonal injury. The primary injury refers to the damage of the initial trauma and often occurs before the paramedics arrive at the scene. In some cases, this is a small core that becomes ischemic due to loss of blood flow and is surrounded by a "penumbra" of tissue where local blood flow is substantially reduced, compromising neuronal function but not viability. Approximately 40% of TBI patients deteriorate in the days after the initial injury,[4] due to the onset of secondary injury, at a time when the patient is being monitored in the intensive therapy unit (ITU). Secondary injuries can be caused by ischemia, cerebral hypoxia, cytotoxic cerebral edema, raised intracranial pressure, neurovascular edema, and spreading depolarization waves (SDs).

The spontaneous occurrence of SDs in the injured human brain were first observed by the Strong/Boutelle collaboration.[5] The mass depolarization of cells, first described by Leao in 1944,[6] propagates like a wave over the cortex, leading to temporary failure of ion homeostasis with a rise in extracellular potassium and intracellular sodium and calcium and disruption of cortical function. The depression of the electrical signal coincides with a transient increase in blood flow and changes in metabolism due to the high demand of energy needed to repolarize the cells.[7] SDs have been shown to occur in 56% of TBI patients, often in stereotyped clusters[8] and with a high indicidence in other types of brain injury.[9] They have been associated with ischemic damage[10] and the onset of neurological deficits.[11] A study by Murray et al. showed that the commonly used clinical covariates, such as age, pupil reactivity, level of hypoxia, and motor score, only explain 30% of the variance in TBI outcome.[12] Results obtained by the Co-Operative Study on Brain Injury Depolarisations (COSBID) group, show that the occurrence of SDs independently predicts poor patient outcome, and is a better indicator than any of the currently used factors.[13]

In experimental models, SD waves can be detected electrophysiologically or real-time imaging of blood flow can be used to map the path of SD waves. High temporal resolution is required as the SD wave takes a few minutes to pass any particular point. Real time measurement of cerebral blood flow (CBF) using laser speckle contrast imaging (LSI) has been used to study SD propagation under both normal[14,15] and

Special Issue: Monitoring Molecules in Neuroscience

Received: February 13, 2013
Accepted: April 10, 2013
Published: April 10, 2013

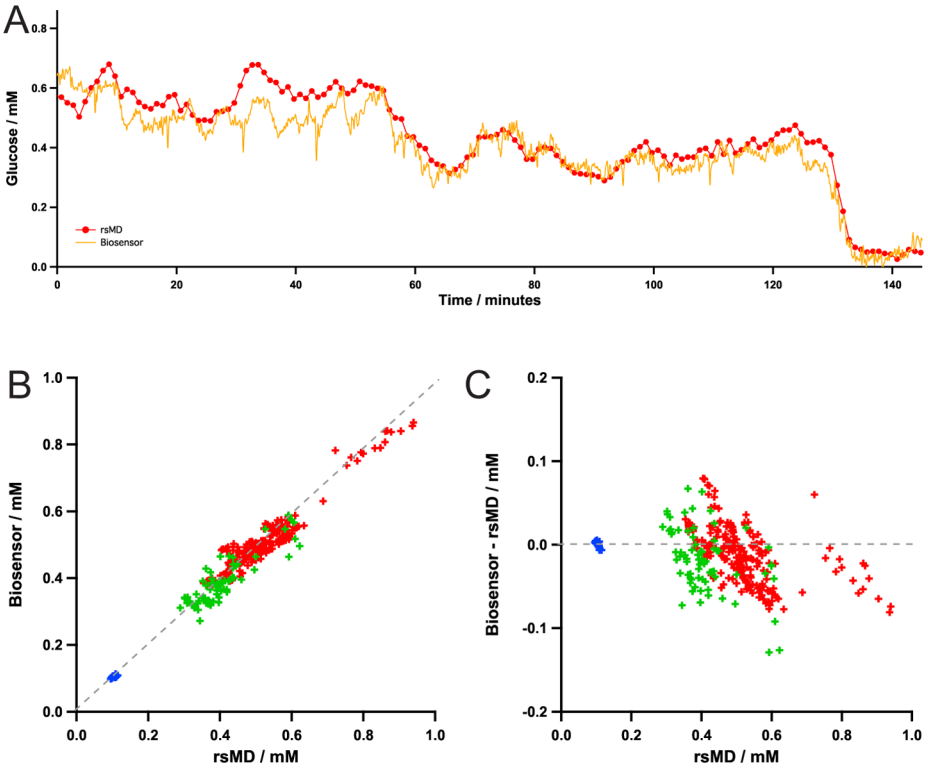

Figure 1. Glucose biosensor validation. (A) Comparison of glucose rsMD to biosensor data over the course of an procedure. Data was individually time-aligned and analyzed using calibrations of sensors before being overlaid. The levels vary over the duration of the procedure and finally fall to near zero after euthanasia at 107 min. (B) Comparison of glucose biosensor and rsMD data. (C) The mean difference in data measurement as a function of the rsMD glucose value. From these data, on average across the concentration range, the concentration determined by the biosensor was marginally, but significantly lower than that determined by rsMD (-16.6 ± 44 μM, $p = 0.0001$, $n = 356$).

ischemic[16−18] conditions. It has been shown to be a good tracker of SD waves[16,19] and is a semiquantitative measure of dynamic CBF.[20] LSI has high spatial and temporal resolution (30 μm and 1 s, respectively), providing a high-resolution map of the evolution of cerebral blood flow.[19] The number of depolarizations and the clustering of these events are associated with the growth of the infarct area[21−23] due to ischemic damage in the penumbra.[16,17] It has also been shown that SD waves may cycle around the site of injury, possibly explaining the repetition at regular intervals seen also in some patients.[15]

Using MRI and PET imaging studies in patients, a UCLA group has shown that during a persistent metabolic crisis, the lactate/pyruvate ratio increases, and this has been shown to be indicative of tissue atrophy at 6 months with oxidative brain metabolism playing a central role.[24,25] Studies of TBI patients cortical glucose levels using classical microdialysis with hourly samples, have indicated that depletion of brain glucose carries a poor prognosis.[26] However, this temporal resolution is insufficient to detect the frequently occurring dynamic changes that challenge the tissue. The metabolic signature of a transient ischemia has been detected using implanted biosensors[27] and online rapid sampling microdialysis (rsMD),[28] as a decrease in glucose levels and increase in lactate levels, typically lasting 2−5 min.[29] Using rsMD in animal studies, such a signature was also found as an SD wave passes a MD probe,[30] leading to an extended reduction in brain glucose. In human studies, rsMD could initially only show a correlation between the number of SD waves and the fall in brain glucose.[31] Improvements in sensitivity of the assay and the development of algorithms to reduce noise[32] have confirmed the chemical signature of SD waves in patients and shown that repetition of the events can drive down the local glucose concentration, to a level where the tissue is no longer viable.[29] However, with the 1 min temporal resolution coupled to the small (20−50 μM), rapid decreases in brain glucose, the temporal resolution of rsMD is at its limit. To study the temporal profile of SDs further, two important challenges remain: to know the start of the SD event in the microdialysis data and to detect the metabolism changes with high temporal resolution. We have addressed the first with an online potassium ion selective electrode (ISE)[33] and the second with an online glucose biosensor. For increased time-resolution, the novel glucose biosensor together with the potassium ISE were integrated in a microfluidic platform designed to monitor the neurochemical effects of SD waves.

1. RESULTS AND DISCUSSION

1.1. Biosensor Characterization. The glucose biosensors have an average sensitivity of $3.9 \pm 0.6 \times 10^3$ nA/mM/cm^{-2} ($n = 15$) and a $T_{90\%}$ of 3.1 ± 1.3 s ($n = 15$). All results are presented as mean $\pm$ standard deviation. The main sources of noise are interference from the magnetic stirrer and the injection of known glucose concentration used to assess the sensor performance during calibrations. The inherently fast time responses of these sensors allow for measurements with a temporal resolution on the order of seconds.

Although the sensor is held at a 0.7 V (vs AglAgCl) throughout the experiment, interference from other electroactive species, namely, ascorbic acid and dopamine, is not an issue due to the protection provided from the poly(phenol) film used. Using a similar needle electrode, the interference

dx.doi.org/10.1021/cn400047x | ACS Chem. Neurosci. 2013, 4, 799−807

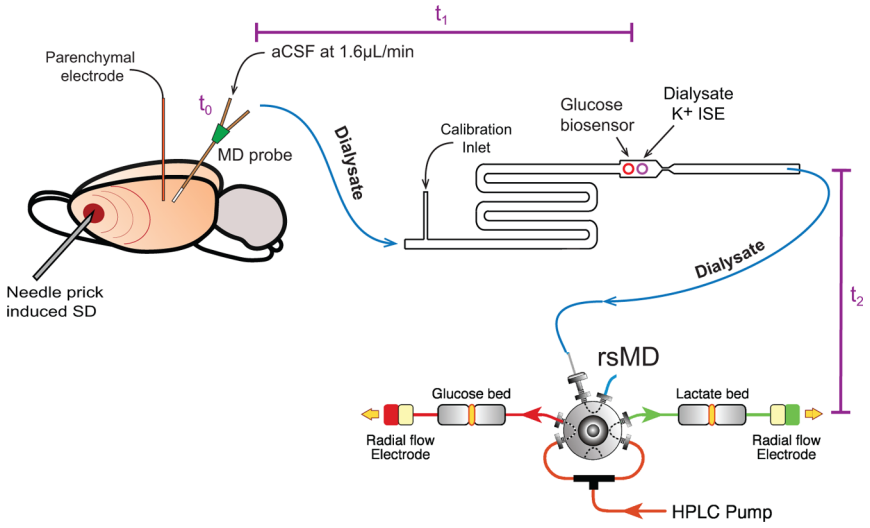

Figure 2. Translational setup. Not to scale. t_0 is the time the event hits the MD membrane. t_1 is the time delay before the dialysate, representative of the event, reaches the sensors (on average 4 min). t_2 is the dialysate transfer time from the sensors to rsMD (on average 15 min). A potassium ISE and a glucose biosensor are placed within a chamber of 68 nL volume. Dialysate is passed to rsMD for flow injection analysis of glucose and lactate.

through this film has been previously assessed as negligible for an ATP sensor detecting smaller changes.[34]

1.2. Biosensor Validation. To ensure that the online biosensors were capable of detecting biologically relevant concentrations of glucose in brain dialysate, the results from the glucose biosensor within the microfluidic chip were compared to the results of rsMD which analyzed the same dialysate sample. Figure 1A shows that the results of the two analysis techniques overlaid, after being individually analyzed and time-aligned. This data set shows levels of glucose recorded in vivo during 2 h. At 60 min, a blood clot was removed and at 127 min, the animal was euthanized, and glucose levels fell to near zero. Glucose concentrations are fluctuating over the course of the experiments, with both monitoring techniques showing parallel changes, indicating good agreement between the microfluidic glucose biosensor and rsMD glucose.

Figure 1B shows the comparison of three online biosensors to the equivalent rsMD data. If the glucose measurement was that of blood, it would be appropriate to use a Clarke error grid.[35] However, for continuous glucose monitoring, the relative timing of paired results during a dynamic change is very important.[36] As both monitoring systems used in the current study analyze the same dialysate stream from the same extracellular tissue space, the mean difference between the two techniques provides a better estimation of sensor performance. This is shown in Figure 1C. On average, there is a slight bias for the biosensor to report lower values compared to that of rsMD ($-16.6 \pm 44\ \mu M$, $p = 0.0001$, $n = 356$). However, analysis shows that the least squared regression slope is not significantly different from zero.

1.3. Multimodal Approach to SD. A multimodal approach was taken to investigate spreading depolarizations and fully test the microfluidic platform. All the recordings were individually calibrated and time aligned to t_0, the time when the SD wave reaches the MD probe. Figure 2 shows the experimental setup used. The t_0, t_1, and t_2 values were determined experimentally as explained in the Methods section.

An overview of all the measurements taken is shown in Figure 3. Successful induction of the SD wave was confirmed by a DC negative shift and a transient suppression of the ECoG activity (Figure 3B), which are characteristic of cellular depolarization. The propagation of the SD wave could be tracked by LSI; the passage of a hyperemic wave at a speed of

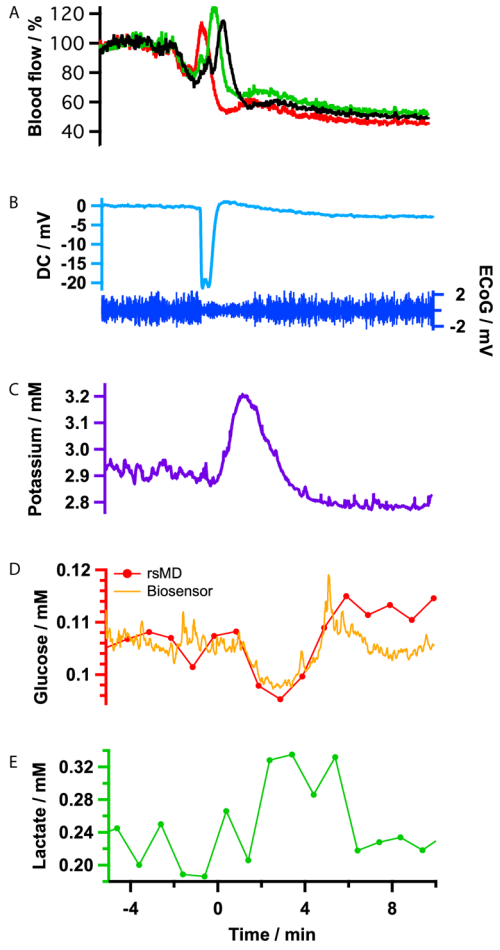

Figure 3. Multimodal response to an SD wave. (A) Blood flow at three different ROIs in progressing distance (red, green, black) from the site of the needle prick. (B) DC potential (light blue) and ECoG (dark blue). (C) Microdialysate potassium. (D) Glucose readings from rsMD (red) and dialysate biosensor (yellow). (E) rsMD lactate.

dx.doi.org/10.1021/cn400047x | ACS Chem. Neurosci. 2013, 4, 799−807

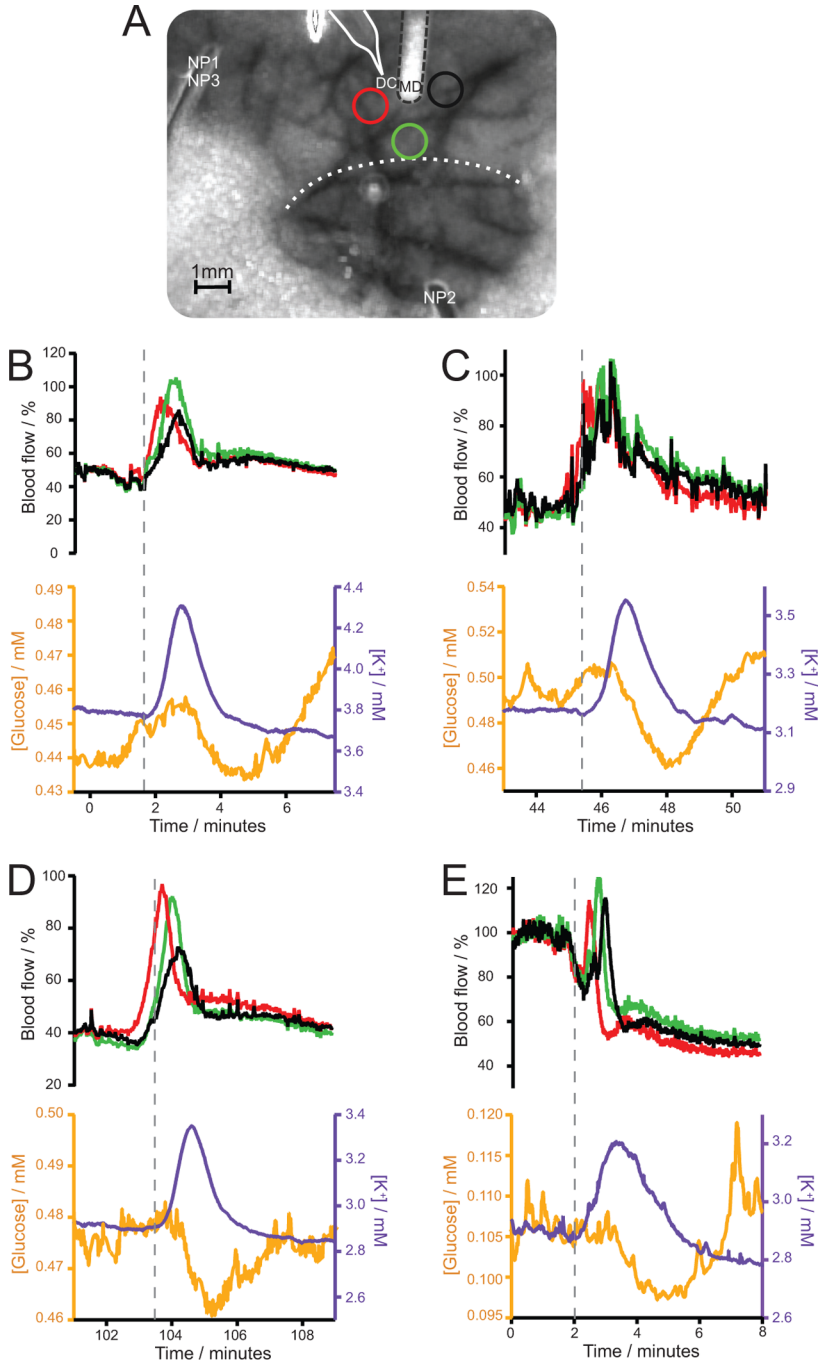

Figure 4. Microfluidic sensors. Panel (A) is a laser speckle image showing the left hemisphere through a thinned skull. The sites for needle prick stimuli are indicated (NP1,2,3) and the positions of the intraparenchymal microelectrode (DC) and microdialysis probe (MD) are also marked. Three circular ROIs were used to analyze the blood flow response around the implanted measurement sites. The color of the circle indicates the trace seen in the blood flow graphs. The dotted line indicates the wavefront of the SD wave elicited by the second needle prick at the time of the still. Panels (B–D) show the response of the microfluidic sensors of needle pricks conducted in the same rat under propofol (NP1,2,3). Panel (E) shows the responses from a different rat under isoflurane (NP1). The gray dotted lines in (B–E) show the moment the SD wave hits the MD probe as indicated by the change in potassium.

4.4 mm/min passed the parenchymal microelectrode, and the MD probe was verified (Figure 3A). By using such a multimodal approach, we can be sure that changes in concentrations given by the microfluidic sensors are a response to a true event taking place in the brain tissue sampled by the MD probe, which gives confidence in the interpretation of the online MD sensor data.

The on-chip MD potassium ISE response is shown in Figure 3C. An increase in extracellular potassium is typical for an SD wave and can be here observed in the microdialysate, given the limitations of microdialysis sampling and dispersion. A detailed study on MD online potassium measurement can be found in ref 33. The glucose levels, as recorded by both the microfluidic biosensor and rsMD, are compared in Figure 3D. The concentrations correlate very well before and during the SD.

dx.doi.org/10.1021/cn400047x | ACS Chem. Neurosci. 2013, 4, 799–807

After the SD, the rsMD trace is slightly higher, though the difference is within the error calculated for Figure 1C. During the SD, the concentration of glucose decreases by 12 μM in both data sets. The rsMD lactate data is shown in Figure 3E, where levels increase as the SD wave passes, as observed previously in experimental and clinical monitoring of SD with rsMD.[14,29]

1.4. Microfluidic Sensor Data: Neurometabolic Coupling. To better appreciate the advantage of the finer time-resolution of the glucose biosensor (as opposed to the minute time-resolution of the rsMD), the responses of the microfluidic sensors and of the near real-time CBF measurements are shown in Figure 4. Four sections of data are shown, each being the response to a different needle prick, from two rats, one under propofol (Figure 4B–D) and the other under isoflurane (Figure 4E). In all cases, blood flow, on-chip potassium and glucose biosensor responses have been time-aligned (see Methods section). A propagating hyperaemia is seen in the laser speckle data with each needle prick, indicating a SD wave passing through the area where the MD probe was implanted at a speed of 4.4 mm/min, typical of first SD wave speeds.[37] This indicates that the presence of the MD probe did not alter the propagation direction or speed of the SD wave. Furthermore, the hyperaemic peak coincides with the onset of increase in extracellular potassium, as detected by the microfluidic ISE. Once the hyperemia has passed, the potassium levels begin to fall to near baseline, indicating repolarization of the neuronal cells. In each case the glucose biosensors show a transient decrease in the local concentration. This is true for all four NP data sets as seen in Figure 4. Interestingly, in our multi-needle-prick model, brain glucose and CBF had all recovered to their baseline value before the changes induced by the SD wave (baseline [glucose] $\approx$ 0.47 mM under propofol, 0.105 mM under isoflurane, and CBF $\approx$ 50% under propofol and 100% under isoflurane).

Given microdialysis recovery (estimated in vitro as 32–33%), these baseline values are in accordance with interstitial glucose concentrations found in the literature to be in the order of 2–3 mM in anaesthetised animals.[28] Although the higher cerebral blood flow under isoflurane would lower the in vivo recovery of a species not present in the blood,[38] for glucose this would not be the case as the blood flow is the source of brain glucose. The extracellular level of glucose is a balance between this source and the local utilization. Our lower baseline dialysate glucose concentration under isoflurane compared to propofol is mainly due to the anesthetic, since propofol increases brain glucose by 50% compared to isoflurane,[39] and partly due to a slight difference in the in vivo recovery of the MD probe. Given the small sample of animals used in this study, we cannot conclude on a significant quantitative effect of anesthesia on brain glucose concentrations. The temporal relationship between microdialysis potassium and glucose is however not influenced by the anesthetics.

In one animal, after the second needle prick, there was a transient drop in blood pressure (down to 48 mmHg), which triggered the spontaneous propagation of a second SD wave 6 min after the induced SD (shown in Figure 5). Here, in contrast to the SD initiated via the needle prick, the glucose concentration decreases immediately as the SD passes the MD probe.

The temporal coupling between membrane cell repolarization, cerebral blood flow, and glucose utilization can be seen for the first time thanks to our subminute temporal resolution. The

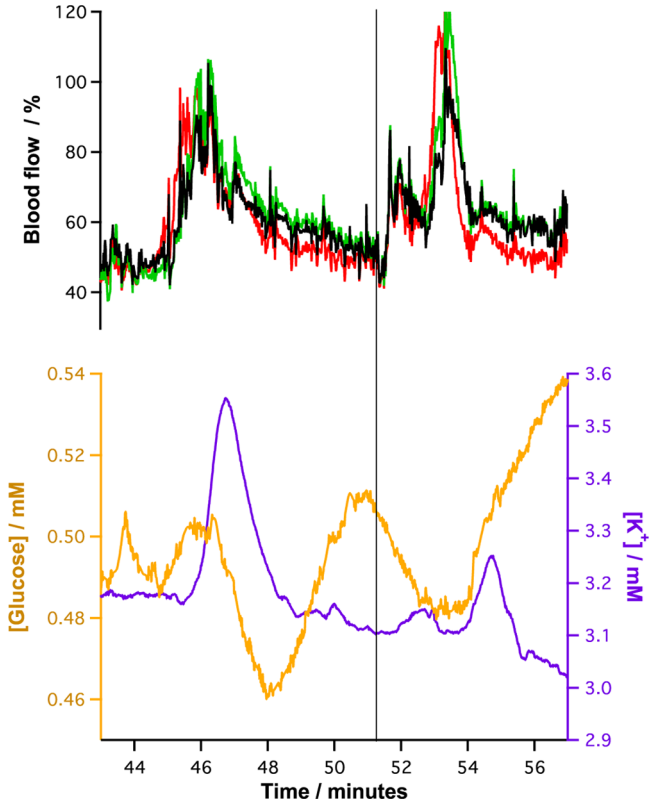

Figure 5. Spontaneous SD wave following a spontaneous drop in blood pressure. Top graph shows the blood flow; bottom graph shows the online glucose (orange) and potassium (purple) data. The first SD was induced from a needle prick. The second SD wave is a spontaneous wave, likely to be caused by a drop in blood pressure (gray line indicates when the blood pressure was at its lowest).

microfluidic data from the four needle pricks was indeed analyzed more closely by looking at just the microdialysate potassium and glucose levels, as seen in Figure 6. Allocating the point of change in potassium as $t = 0$, all potassium and glucose concentration changes were aligned. The background level of each is also removed and the relative changes ($\Delta[K^+]$ and Δ[glucose]) and timings can be closer assessed. In the top graph, all of the potassium changes are overlaid. Clearly, each SD wave causes a transient increase in MD potassium concentrations, characteristic of transient extracellular potassium changes observed with in situ electrodes.[33,40] In the bottom graph the glucose concentration changes are shown for the same four needle pricks. The changes are all small and all negative from the baseline. The magnitude of the changes in glucose seen here are of similar magnitude to the changes seen in patient data using rsMD.[29] Interestingly, all four needle pricks show some delay in the decrease of local concentration compared to the start of the response of potassium. Note that the glucose biosensor was always positioned upstream of the potassium sensor. In calibrations, the biosensor responded to the change in concentrations first (data not shown) and this slight delay was taken into account when time-aligning the two sensors. Therefore we can rule out this delay being due to mass transport effects. There is thus a 62 $\pm$ 24.8 s (n = 4) delay between the onset of the potassium and onset of the glucose responses, which is of physiological origin. This time delay is too short to be seen using the one minute sampling of rsMD. The decrease in glucose actually coincides with the reversal of

dx.doi.org/10.1021/cn400047x | ACS Chem. Neurosci. 2013, 4, 799–807

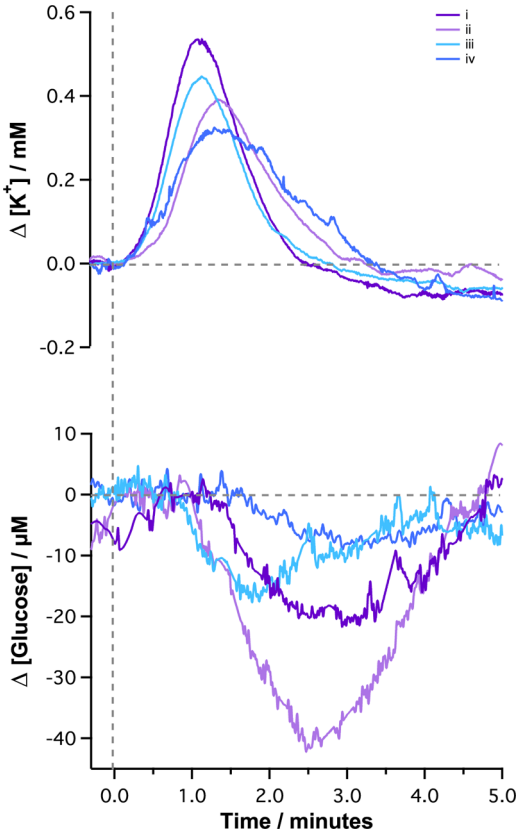

Figure 6. Assessment of glucose and potassium changes. Time $t = 0$ is the point where MD potassium levels start to increase. Potassium and glucose levels were time aligned to each other using calibration data (see Methods section). Background levels of both potassium and glucose have been removed. (i)−(iii) are traces (B)−(D) of Figure 5, respectively, and were conducted under propofol. (iv) is trace (E) of Figure 5 where isoflurane was the anesthesia.

the potassium trend, as seen in Figure 6. Re-establishment of the ionic gradients after depolarization requires indeed much energy to power the pumps to actively transport ions across the cell membranes, and therefore the local demand for glucose increases.

This coupling between restoration of ion homeostasis and increased metabolic demand can be for the first time unambiguously shown thanks to the very high-temporal resolution of both the ISE and the glucose biosensor, which analyze the same dialysate sample. Remarkably, despite a clear hyperemia associated with each SD wave (see Figure 4B−E), which presumably increases the supply of glucose and oxygen from the blood, extracellular glucose drops. This has been previously observed in cats using rsMD.[14] It can therefore be concluded that the drop in cerebral glucose, observed here in rats, and elsewhere in cats and in brain injury patients, is the *consequence* of the increased energy demand for cell repolarization, demand which is not met by local supply from the blood.

2. CONCLUSION

This study has shown the development of microfluidic glucose biosensors to be instrumental in the development of a clinical monitoring system. In this study, we used an in vivo needle prick model, as a translational replica of a "mini" traumatic brain injury to assess the performance of the new online microdialysis biosensors and investigate neuro-metabolic coupling in response to an SD wave.

The glucose biosensor was validated against rsMD glucose with excellent results. A potassium sensor was additionally placed on-chip within the analysis chamber to analyze the sample of dialysate. Thanks to the fast time responses and continuous analysis of microdialysate streams, this study has allowed an unambiguous insight into the timing of the chemical events that occur during an SD wave, a distinct advantage over the currently used flow injection system. It was indeed found that the decrease in glucose only occurred as the cells started repolarizing, as indicated by the coincidence of the onset of the glucose fall with the onset of the recovery of potassium. It was concluded that when the cells begin to repolarize after the passage of an SD wave, the supply of metabolic substrates by the blood does not match the increased demand for repolarization and so the local glucose concentration is seen to fall. On-going optimization of the microfluidic manifold and sensors[41] for clinical use will drive this work forward. The small sample size for the animal data in the current study restricts our ability to analyze the mechanism of changes in detail. However, the findings presented here highlight the potential that the microfluidic system holds for the monitoring of brain injury patients by allowing the analysis of multiple analytes in real-time within the same low-volume dialysate sample. With the very high temporal resolution this provides, the cause/consequence questions can begin to be answered. More widely, this technology could allow the detection and study of transient ischemia or functional activation.

3. METHODS

3.1. Electrode Fabrication. The glucose biosensors in this paper are based upon the combined needle electrodes,[34] a photograph of which is shown in Figure 7A. Briefly, 50 μm Teflon insulated platinum wire (A-M Systems Inc.) and 50 μm polyester insulated silver wire (AM systems) were threaded through a 27G hypodermic needle. The wires were stripped of their insulator using a lighter to expose the metal wire. Electrical wire was glued using conductive silver epoxy glue (RS Components). Epoxy resin (Robnor resins, CY1301 and HY1300) was used to fill the internal volume of the needle and secure the wires in place. Once the epoxy had cured, the sharp end of the needle was cut using a diamond saw (Buehler) to expose the microelectrodes. The ends were polished using alumina slurries finishing with 0.05 μm. The silver disc was chloridized by placing in Referencing Solution (BAS) for 5 s, to create AglAgCl reference electrode. Cyclic voltammetry was used to assess the surface of the electrode. The working electrode consisted of a 50 μm diameter platinum disc electrode. A scanning electron microscopy (SEM) image of the polished needle tip can be seen in Figure 7B.

3.2. Glucose Biosensor Fabrication. All biosensors were controlled via a lab built potentiostat feeding into a Powerlab 16/35 running LabChart Pro (AD Instruments). The combined electrode was placed in a solution containing 50 mM Phenol and 4 mg/mL glucose oxidase. The pH of the solution was buffered to pH 7.2. The electrode was placed in the enzyme solution for 10 min. Then under potentiostatic control, the working electrode was held at 0 V for 20 s, polarized to 0.9 V for 15 min for electropolymerization, and then held at 0 V for 20 s. The biosensor was gently rinsed with deionized water and stored dry overnight at 4 °C before use. The biosensors were characterized in a beaker containing phosphate buffer solution (PBS), which was highly stirred. Aliquots of a concentrated glucose solution were added to the PBS using a glass syringe (Hamilton), to create known step changes in concentration in the bulk media. Figure 7C shows the raw data of a 100 μM step change of glucose. The limit of detection, calculated as 3x the standard deviation of the baseline signal,

dx.doi.org/10.1021/cn400047x | ACS Chem. Neurosci. 2013, 4, 799−807

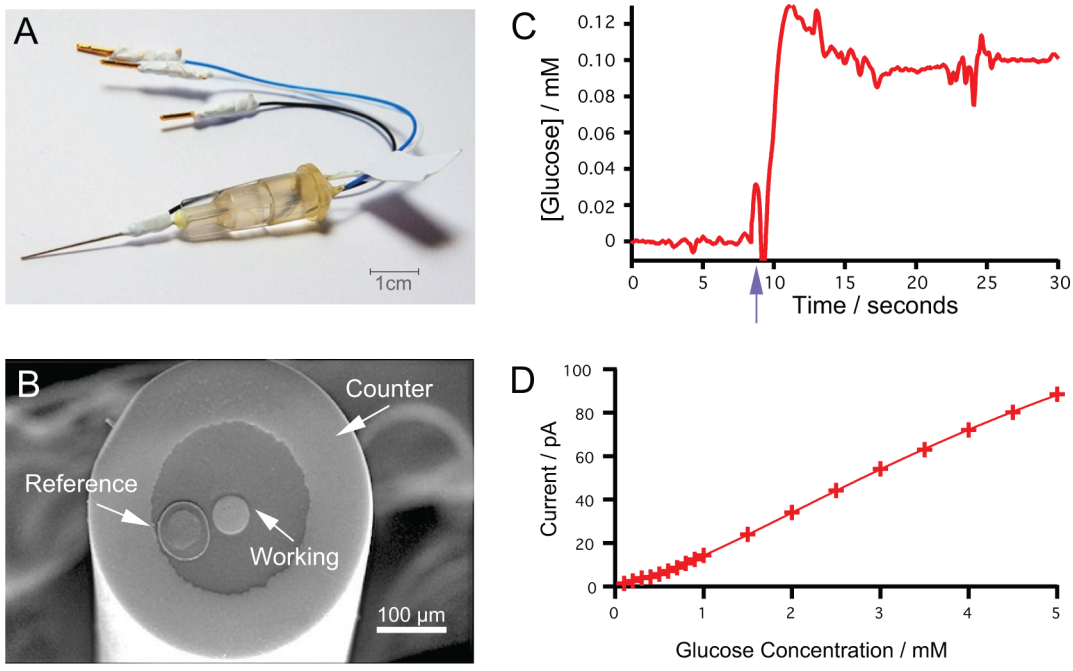

Figure 7. Sensor design. (A) Photograph of combined needle electrode. (B) SEM image of the needle tip. The working electrode is a 50 μm platinum/iridium disc; the reference electrode is formed by chloridizing the 50 μm silver disc to get Ag|AgCl; the counter electrode is the stainless steel shaft of the hypodermic needle. (C) Raw data calibration using a 50 μm glucose biosensor. Biosensor is held at a constant potential of 0.75 V. Aliquots of glucose standard are added and current response recorded. Purple arrow indicates the change in glucose concentration from 0 to 100 μM. (D) Calibration indicating current against glucose concentration using a 50 μm glucose biosensor. Data is fitted with the Hill equation giving an apparent K_m value of 11.35 ± 0.075 mM.

is 1.5 μM. Figure 7D shows a calibration within the brain physiological range. The data has been fitted with the Hill equation using IgorPro.

3.3. In Vivo Experiments. All animal procedures were carried out in accordance with the German Laws for Animal Protection and institutional guidelines. Two male Wistar rats were anesthetized with isoflurane (5% induction, 1.5−2% maintenance) in a 70%:30% nitrous oxide/oxygen mixture during all surgical procedures. Rectal temperature was maintained at 37 °C using a servo-controlled heating blanket. The left femoral artery was cannulated for continuous blood pressure recording and hourly arterial blood gases measurements. The left frontal and parietal bones were exposed and thinned out to transparency using a dental drill. Drilling was performed under continuous saline irrigation to prevent heat injury. The cavity formed covered most of the left cerebral cortex and provided a field of view of ~10 × 7 mm for LSI. Two small burr-holes were drilled into the frontal and parietal cortex for subsequent needle pricks at two different sites (see Figure 4A). Two small durectomies were drilled at 3.5 mm posterior and 3.5 mm lateral to Bregma and 4 mm posterior and 3.5 mm lateral to Bregma for the parenchymal electrode and the microdialysis (MD) probe, respectively. The durectomies were placed in areas devoid of major blood vessels and at the edge of the field of view so as to limit artifacts for LSI. The distance between the microelectrode and the MD probe (≈0.5 mm distance) was as small as possible to ensure simultaneity of the events at both measurement sites.

After all surgical procedures were completed, LSI was started and continued uninterrupted during the whole duration of the experiments. The LSI method was implemented as previously described.[15,19] After baseline imaging, the MD probe (MAB 6.14.2, Microbiotech, Sweden) was implanted using a piezoelectric motor at a rate of 5 μm/s, while being perfused with aCSF at a rate of 1.6 μL/min. The probe was implanted obliquely to full membrane length (2 mm), so as to ensure maximal sampling from cortical tissue. The MD probe outlet was connected directly to a microfluidic analysis chip containing first a glucose biosensor and then a potassium ISE.[33] The dialysate stream was then fed into the rsMD valve for flow injection analysis of glucose and lactate. A schematic of the procedure setup is shown in Figure 2. A glass microelectrode (2.5−3 μm tip diameter) was then implanted at a depth of 500 μm. Direct current (DC) and electrocorticogram (ECoG) were measured versus a subcutaneous sintered Ag/AgCl wire electrode that served as a reference. The animal was earthed to the instrumentation ground.

A waiting period of 45 min followed implantations, during which all measured parameters (arterial blood pressure, CBF, brain glucose, lactate and potassium, DC, and ECoG) stabilized to normal physiological values. One animal was maintained under isoflurane (1.5%), and the other animal was switched to propofol (38 mg/kg/h infusion via tail vein), an intravenous anesthetic commonly used in ITU for TBI patients.[42] The effect of propofol compared to isoflurane on CBF and SD waves has been discussed elsewhere.[43,44] After stabilization of all parameters, a first needle prick was performed on the frontal cortex. The needle prick model can be understood as a mechanically induced focal traumatic injury, causing one single SD wave.[45,46] After 1 h, when CBF had recovered to its baseline values, a second SD wave was elicited by needle prick on the parietal cortex. When the animal conditions allowed it, a third needle prick was performed 1 h later on the frontal cortex, triggering a single SD wave. In one animal, after the SD wave caused by the second needle prick, a transient drop in blood pressure was observed (down to 48 mmHg), which triggered the spontaneous propagation of a second SD wave (see Figure 5). At the end of the experiment, the animals were euthanised by intravenous injection of a high concentration of potassium chloride (3 M KCl).

3.4. Data Analysis. Speckle contrast images were analyzed for CBF by placing regions of interest (ROIs) of 1 mm diameter in areas devoid of major blood vessels. Three ROIs were positioned around the implanted electrode and MD to capture the SD wave as it approaches and passes the probes (see Figure 4). CBF values are here reported relative to baseline CBF under isoflurane taken as 100% CBF. Electrophysiological data from the parenchymal microelectrode were digitized at 250 Hz and low-passed filter for DC and high -pass filtered for ECoG (0.1 Hz cutoff frequency in both cases). The online MD data were analyzed independently and blindly for rsMD glucose and lactate in Cologne and for the online potassium and glucose sensors in

dx.doi.org/10.1021/cn400047x | ACS Chem. Neurosci. 2013, 4, 799−807

London. Data were denoized using our previous published algorithms.[32] Before each in vivo experiment, an in vitro MD recovery experiment was conducted, where the MD probe was moved between known solutions at known times. This not only checked the functionality of the MD probe but also allowed the time difference between the known responses of the different analysis techniques to be measured. If t_0 is the time at which a change occurred at the MD probe membrane, t_1 is the length of time for this change to be detected at the microfluidic sensors and t_2 is the time to move the dialysate from the sensors to being injected into the rsMD valve, as seen in Figure 2. Once these values are known, all the individual data sets can be aligned to the same time point, t_0. All results presented in the text have been time-aligned between the different analysis techniques.

AUTHOR INFORMATION

Corresponding Author

*E-mail: m.boutelle@imperial.ac.uk.

Author Contributions

‖M.L.R. and D.F. contributed equally to this work.

Author Contributions

M.L.R. and D.F. contributed equally to this work and prepared the manuscript. M.L.R., D.F., and C.L.L. carried out the experimental work and analyzed the data. M.T. performed all the surgery. X.N. aided design and fabrication of microfluidic chips. R.G. and M.G.B. participated in the design and interpretation of the experiments and finalization of the manuscript.

Funding

The authors thank the Wellcome Trust/DOH HICF fund, Alexander von Humboldt Foundation, and the BBSRC.

Notes

The authors declare no competing financial interest.

ACKNOWLEDGMENTS

We would like to thank Paula Gabel for excellent technical support.

REFERENCES

(1) Neurology, L. (2010) Traumatic brain injury: time to end the silence. *Lancet Neurol. 9*, 331.

(2) Whitfield, P., Thomas, E., Summers, F., Whyte, M., and Hutchinson, P. (2009) *Head injury-a multidisciplinary approach*; Cambridge University Press: New York; page 309.

(3) Finkelstein, E., Corso, P., and Miller, T. (2006) *Incidence and economic burden of injuries in the United States*; Oxford University Press: Oxford.

(4) Narayan, R., Michel, M., Ansell, B., Baethmann, A., Biegon, A., Bracken, M., Bullock, M., Choi, S., Clifton, G., Contant, C., Coplin, W., Dietrich, W., Ghajar, J., Grady, S., Grossman, R., Hall, E., Heetderks, W., Hovda, D., Jallo, J., Katz, R., Knoller, N., Kochanek, P., Maas, A., Majde, J., Marion, D., Marmarou, A., Marshall, L., McIntosh, T., Miller, E., Mohberg, N., Muizelaar, J., Pitts, L., Quinn, P., Riesenfeld, G., Robertson, C., Strauss, K., Teasdale, G., Temkin, N., Tuma, R., Wade, C., Walker, M., Weinrich, M., Whyte, J., Wilberger, J., Young, A., and Yurkewicz, L. (2002) Clinical trials in head injury. *J. Neurotrauma 19*, 503−557.

(5) Strong, A., Fabricius, M., Boutelle, M., Hibbins, S., Hopwood, S., Jones, R., Parkin, M., and Lauritzen, M. (2002) Spreading and synchronous depressions of cortical activity in acutely injured human brain. *Stroke 33*, 2738−2743.

(6) Leao, A. (1944) Spreading depression of activity in the cerebral cortex. *J. Neurophysiol. 7*, 359.

(7) Lauritzen, M. (1994) Pathophysiology of the migraine aura. *Brain 117*, 199−210.

(8) Fabricius, M., Fuhr, S., Bhatia, R., Boutelle, M., Hashemi, P., Strong, A., and Lauritzen, M. (2006) Cortical spreading depression and peri-infarct depolarization in acutely injured human cerebral cortex. *Brain 129*, 778−790.

(9) Dohmen, C., Sakowitz, O., Fabricius, M., Bosche, B., Reithmeier, T., Ernestus, R., Brinker, G., Dreier, J., Woitzik, J., Strong, A., and Graf, R. (2008) Spreading depolarizations occur in human ischemic stroke with high incidence. *Ann. Neurol. 63*, 720−728.

(10) Dreier, J., Major, S., Manning, A., Woitzik, J., Drenckhahn, C., Steinbrink, J., Tolias, C., Oliveira-Ferreira, A., Fabricius, M., Hartings, J., Vajkoczy, P., Lauritzen, M., Dirnagl, U., Bohner, G., and Strong, A. (2009) Cortical spreading ischaemia is a novel process involved in ischaemic damage in patients with aneurysmal subarachnoid haemorrhage. *Brain 132*, 1866−1881.

(11) Dreier, J., Woitzik, J., Fabricius, M., Bhatia, R., Major, S., Drenckhahn, C., Lehmann, T., Sarrafzadeh, A., Willumsen, L., Hartings, J., Sakowitz, O., Seemann, J., Thieme, A., Lauritzen, M., and Strong, A. (2006) Delayed ischaemic neurological deficits after subarachnoid haemorrhage are associated with clusters of spreading depolarizations. *Brain 129*, 3224−3237.

(12) Murray, G., Butcher, I., McHugh, G., Lu, J., Mushkudiani, N., Maas, A., Marmarou, A., and Steyerberg, E. (2007) Multivariable prognostic analysis in traumatic brain injury: results from the IMPACT study. *J. Neurotrauma 24*, 329−337.

(13) Hartings, J., Bullock, M., Okonkwo, D., Murray, L., Murray, G., Fabricius, M., Maas, A., Woitzik, J., Sakowitz, O., Mathern, B., Roozenbeek, B., Lingsma, H., Dreier, J., Puccio, A., Shutter, L., Pahl, C., and Strong, A. (2011) Spreading depolarisations and outcome after traumatic brain injury: a prospective observational study. *Lancet Neurol. 10*, 1058−1064.

(14) Hashemi, P., Bhatia, R., Nakamura, H., Dreier, J., Graf, R., Strong, A., and Boutelle, M. (2008) Persisting depletion of brain glucose following cortical spreading depression, despite apparent hyperaemia: evidence for risk of an adverse effect of Leao's spreading depression. *J. Cereb. Blood Flow Metab. 29*, 166−175.

(15) Nakamura, H., Strong, A., Dohmen, C., Sakowitz, O., Vollmar, S., Sué, M., Kracht, L., Hashemi, P., Bhatia, R., Yoshimine, T., Dreier, J., Dunn, A., and Graf, R. (2010) Spreading depolarizations cycle around and enlarge focal ischaemic brain lesions. *Brain 133*, 1994−2006.

(16) Strong, A., Anderson, P., Watts, H., Virley, D., Lloyd, A., Irving, E., Nagafuji, T., Ninomiya, M., Nakamura, H., Dunn, A., and Graf, R. (2007) Peri-infarct depolarizations lead to loss of perfusion in ischaemic gyrencephalic cerebral cortex. *Brain 130*, 995−1008.

(17) Kumagai, T., Walberer, M., Nakamura, H., Endepols, H., Sué, M., Vollmar, S., Adib, S., Mies, G., Yoshimine, T., Schroeter, M., and Graf, R. (2010) Distinct spatiotemporal patterns of spreading depolarizations during early infarct evolution: evidence from real-time imaging. *J. Cereb. Blood Flow Metab. 31*, 580−592.

(18) Luckl, J., Zhou, C., Durduran, T., Yodh, A., and Greenberg, J. (2009) Characterization of periinfarct flow transients with laser speckle and Doppler after middle cerebral artery occlusion in the rat. *J. Neurosci. Res. 87*, 1219−1229.

(19) Dunn, A., Bolay, H., Moskowitz, M., and Boas, D. (2001) Dynamic imaging of cerebral blood flow using laser speckle. *J. Cereb. Blood Flow Metab. 21*, 195−201.

(20) Strong, A., Hopwood, S., Boutelle, M., Parkin, M., Bezzina, L., Yih-Huei, S., and Dunn, A. (2003) Measuring dynamic changes in perfusion in the penumbra with high spatial and temporal resolution using laser speckle imaging: comparison with indicator clearance. *J. Cereb. Blood Flow Metab. 23*, 300.

(21) Back, T., Ginsberg, M., Dietrich, W., and Watson, B. (1996) Induction of spreading depression in the ischemic hemisphere following experimental middle cerebral artery occlusion: effect on infarct morphology. *J. Cereb. Blood Flow Metab. 16*, 202−213.

(22) Dijkhuizen, R., Beekwilder, J., van der Worp, H., Berkelbach van der Sprenkel, J., Tulleken, K., and Nicolay, K. (1999) Correlation between tissue depolarizations and damage in focal ischemic rat brain. *Brain Res. 840*, 194−205.

(23) Mies, G. (1993) Inhibition of protein synthesis during repetitive cortical spreading depression. *J. Neurochem. 60*, 360−363.
(24) Marcoux, J., McArthur, D., Miller, C., Glenn, T., Villablanca, P., Martin, N., Hovda, D., Alger, J., and Vespa, P. (2008) Persistent metabolic crisis as measured by elevated cerebral microdialysis lactate-pyruvate ratio predicts chronic frontal lobe brain atrophy after traumatic brain injury. *Crit. Care Med. 36*, 2871−2877.
(25) Xu, Y., McArthur, D., Alger, J., Etchepare, M., Hovda, D., Glenn, T., Huang, S., Dinov, I., and Vespa, P. (2009) Early nonischemic oxidative metabolic dysfunction leads to chronic brain atrophy in traumatic brain injury. *J. Cereb. Blood Flow Metab. 30*, 883−894.
(26) Vespa, P., McArthur, D., O'Phelan, K., Glenn, T., Etchepare, M., Kelly, D., Bergsneider, M., Martin, N., and Hovda, D. (2003) Persistently Low Extracellular Glucose Correlates With Poor Outcome 6 Months After Human Traumatic Brain Injury Despite a Lack of Increased Lactate: A Microdialysis Study. *J. Cereb. Blood Flow Metab. 23*, 865−877.
(27) Hu, Y., and Wilson, G. (1997) A temporary local energy pool coupled to neuronal activity: Fluctuations of extracellular lactate levels in rat brain monitored with rapid-response enzyme-based sensor. *J. Neurochem. 69*, 1484−1490.
(28) Caesar, K., Hashemi, P., Douhou, A., Bonvento, G., Boutelle, M., Walls, A., and Lauritzen, M. (2008) Glutamate receptor-dependent increments in lactate, glucose and oxygen metabolism evoked in rat cerebellum in vivo. *J. Physiol. 586*, 1337−1349.
(29) Feuerstein, D., Manning, A., Hashemi, P., Bhatia, R., Fabricius, M., Tolias, C., Pahl, C., Ervine, M., Strong, A., and Boutelle, M. (2010) Dynamic metabolic response to multiple spreading depolarizations in patients with acute brain injury: an online microdialysis study. *J. Cereb. Blood Flow Metab. 30*, 1343−1355.
(30) Hopwood, S., Parkin, M., Bezzina, E., Boutelle, M., and Strong, A. (2005) Transient changes in cortical glucose and lactate levels associated with peri-infarct depolarisations, studied with rapid-sampling microdialysis. *J. Cereb. Blood Flow Metab. 25*, 391−401.
(31) Parkin, M., Hopwood, S., Jones, D., Hashemi, P., Landolt, H., Fabricius, M., Lauritzen, M., Boutelle, M., and Strong, A. (2005) Dynamic changes in brain glucose and lactate in pericontusional areas of the human cerebral cortex, monitored with rapid sampling on-line microdialysis: relationship with depolarisation-like events. *J. Cereb. Blood Flow Metab. 25*, 402−413.
(32) Feuerstein, D., Parker, K., and Boutelle, M. (2009) Practical Methods for Noise Removal: Applications to Spikes, Nonstationary Quasi-Periodic Noise, and Baseline Drift. *Anal. Chem. 81*, 4987−4994.
(33) Leong, C., Feuerstein, D., Takagaki, M., Rogers, M., Laaser, T., Bhatia, R., Backes, H., Graf, R., and Boutelle, M.. (2013) On-line potassium electrode. In preparation.
(34) Patel, B., Rogers, M., Wieder, T., O Hare, D., and Boutelle, M. (2011) ATP microelectrode biosensor for stable long-term in vitro monitoring from gastrointestinal tissue. *Biosens. Bioelectron 26*, 2890−2896.
(35) Clarke, W., Cox, D., Gonder-Frederick, L., Carter, W., and Pohl, S. (1987) Evaluating clinical accuracy of systems for self-monitoring of blood glucose. *Diabetes Care 10*, 622−628.
(36) Oliver, N., Toumazou, C., Cass, A., and Johnston, D. (2009) Glucose sensors: a review of current and emerging technology. *Diabetic Med. 26*, 197−210.
(37) Kudo, C., Nozari, A., Moskowitz, M., and Ayata, C. (2008) The impact of anesthetics and hyperoxia on cortical spreading depression. *Exp. Neurol. 212*, 201−206.
(38) Clough, G., Boutsiouki, P., Church, M., and Michel, C. (2002) Effects of blood flow on the in vivo recovery of a small diffusible molecule by microdialysis in human skin. *J. Pharmacol. Exp. Ther. 302*, 681−686.
(39) Horn, T., and Klein, J. (2010) Lactate levels in the brain are elevated upon exposure to volatile anesthetics: a microdialysis study. *Neurochem. Int. 57*, 940−947.
(40) Vyskocil, F., Kritz, N., and Bures, J. (1972) Potassium-selective microelectrodes used for measuring the extracellular brain potassium during spreading depression and anoxic depolarization in rats. *Brain Res. 39*, 255.
(41) Rogers, M., Leong, C., Niu, X., de Mello, A., Parker, K., and Boutelle, M. (2011) Optimisation of a microfluidic analysis chamber for the placement of microelectrodes. *Phys. Chem. Chem. Phys. 13*, 5298−5303.
(42) Hutchens, M. P., Memtsoudis, S., and Sadovnikoff, N. (2006) Propofol for sedation in neuro-intensive care. *Neurocrit. Care 4*, 54−62.
(43) Feuerstein, D., Takagaki, M., Gramer, M., Manning, A., Endepols, H., Vollmar, S., Yoshimine, T., Strong, A., Backes, H., and Graf, R. (2013) The capacity to raise blood flow in response to increased energy demand defines tissue conditions in brain injury. Submitted.
(44) Takagaki, M., Feuerstein, D., Kumagai, T., Gramer, M., Yoshimine, T., and Graf, R. (2013) Isoflurane suppresses cortical spreading depolarizations compared to propofol - implications for sedation of neurocritical care patients. Submitted.
(45) Richter, F., Rupprecht, S., Lehmenkuhler, A., and Schaible, H. (2003) Spreading depression can be elicited in brain stem of immature but not adult rats. *J. Neurophysiol. 90*, 2163−2170.
(46) Richter, F., Ebersberger, A., and Schaible, H. (2002) Blockade of voltage-gated calcium channels in rat inhibits repetitive cortical spreading depression. *Neurosci. Lett. 334*, 123−126.